

Specificity determinants for lipids bound to β -barrel proteins^S

Amy J. Reese* and Leonard J. Banaszak^{1,†}

Department of Molecular Microbiology,* Washington University School of Medicine, St. Louis, MO; and Department of Biochemistry, Molecular Biology, and Biophysics,[†] University of Minnesota, Minneapolis, MN

Abstract The family of proteins accountable for the intracellular movement of lipids is characterized by a 10-stranded β -barrel that forms an internalized cavity varying in size and binding preferences. The loop connecting β -strands E and F (the fifth and sixth strands) is the most striking conformational difference between adipocyte lipid binding protein (ALBP; fatty acids) and cellular retinoic acid binding protein type I (CRABP I). A three-residue mutation was made in wild-type (WT)-ALBP [ALBP with a three-residue mutation (EF-ALBP)] to mimic CRABP I. Crystal structures of ligand-free and EF-ALBP with bound oleic acid were solved to resolutions of 1.5 Å and 1.7 Å, respectively, and compared with previous studies of WT-ALBP. The changes in three residues of one loop of the protein appear to have altered the positioning of the C₁₈ fatty acid, as observed in the electron density of EF-ALBP. The crystallographic studies made it possible to compare the protein conformation and ligand positioning with those found in the WT protein. Although the cavity binding sites in both the retinoid and fatty acid binding proteins are irregular, the ligand atoms appear to favor a relatively planar region of the cavities. **■** Preliminary chemical characterization of the mutant protein indicated changes in some binding properties and overall protein stability.—Reese, A. J., and L. J. Banaszak. Specificity determinants for lipids bound to β -barrel proteins. *J. Lipid Res.* 2004. 45: 232–243.

Supplementary key words adipocyte lipid binding protein • protein-ligand interaction • ligand binding • oleic acid • retinoic acid

The adipocyte lipid binding protein (ALBP) is a member of a family of 10-stranded β -barrel proteins involved with the intracellular movement of a variety of lipids. All family members with known tertiary structure have the same conformation and approximately the same number of amino acids. However, ligand specificity, affinity, and the locations of the binding site inside the β -barrel cavity can differ significantly within the family. Based on comparisons of a variety of family members and the common factor that all of the ligands have a major hydrophobic

component, questions arise regarding the source of ligand preference. For example, why do some β -barrel family members prefer retinoids and others fatty acids?

Using the conformations of the murine source proteins [1LIB and 1CBR from the Protein Data Bank (PDB)], the amino acid sequence alignment shown in **Fig. 1** was obtained. These two family members were selected because one preferentially binds retinoic acid [cellular retinoic acid binding protein type I (CRABP I; 1CBR)], whereas the other (ALBP; 1LIB) binds a variety of fatty acids. *All trans*-retinoic acid (RA) is an isoprenoid with a relatively rigid conformation, whereas fatty acids generally may have many conformers. In addition, it is clear from previous crystallographic studies that the hydrophobic segment of RA bound to CRABP I is in a different location within the cavity site than are fatty acids in ALBP (1, 2).

Based on the alignment shown in **Fig. 1**, ALBP and CRABP I are 39% identical and ~50% comparable when allowances are made for the usual similarities in some side chains. Using the sequence similarities between ALBP and CRABP I, the conservation of amino acids from species alignments of the CRABPs, and studies of the overlaid structures, several sites on ALBP were identified as the potential sources of the specificity differences. One of them, the clear relocation of the tight turn between the β -strands E and F, became the target of the experiments discussed in this report.

Both the similarities and differences between ALBP and CRABP I are described in the ribbon diagram in **Fig. 2** (stereo). Note that the respective ligands are found on opposite sides of the central binding cavity. The data in **Fig. 2** also demonstrate that the carboxylate head groups in both holo-proteins (indicating crystal structure with ligand bound) point into the cavity away from the helical lid and are located roughly in the same place in the crystal

Abbreviations: ANS, 1-anilinonaphthalene-8-sulfonic acid; apo-, crystal structure without ligand bound; CRABP I, cellular retinoic acid binding protein type I; holo-, crystal structure with ligand bound; OA, oleic acid; PDB, Protein Data Bank; RA, retinoic acid; WT, wild-type.

¹To whom correspondence should be addressed.

e-mail: banas001@umn.edu

S The online version of this article (available at <http://www.jlr.org>) contains an additional four figures.

Manuscript received 12 March 2003 and in revised form 22 October 2003.

Published, *JLR Papers in Press*, November 1, 2003.

DOI 10.1194/jlr.M300113-JLR200

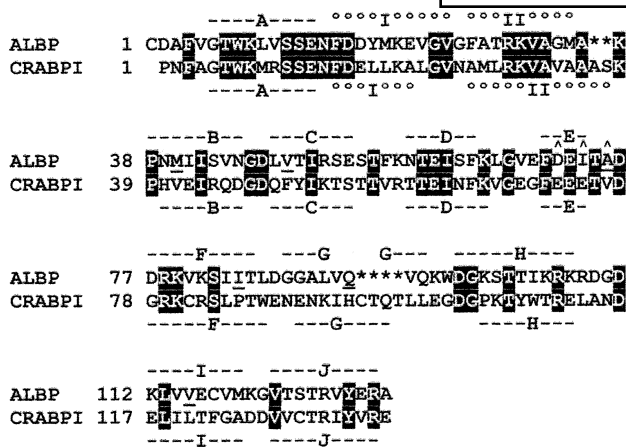


Fig. 1. Amino acid sequence alignment of adipocyte lipid binding protein (ALBP) and cellular retinoic acid binding protein type I (CRABP I). ALBP (accession code P04117) (56) and CRABP I (CAA33509) (57) from mouse sources were aligned based on their crystal structures and least-squares methods. With this alignment, 39% of amino acids are identical and marked in white on black. Asterisks denote alignment gaps. The EF-ALBP mutation sites are indicated with carets above the letters. Numbering is indicated at the beginning of each line for ALBP and CRABP I separately. Secondary structures are highlighted above the ALBP and below the CRABP I sequences: dashes and letters delineate the β -strands, and circles with Roman numerals denote α -helices. ALBP residues that line the cavity and are not conserved in CRABP I are underlined.

structures. Two arginine residues and a tyrosine have been shown to play a role in interacting with the carboxylate of the ligand and hence in partially defining the binding affinity and specificity in both proteins (3). Because the carboxylates of the ligands are found in the same location when bound to both proteins, interaction with the ligand head group is probably not responsible for the discrimination of fatty acids versus retinoids. This led to the search for other determinants of binding specificity.

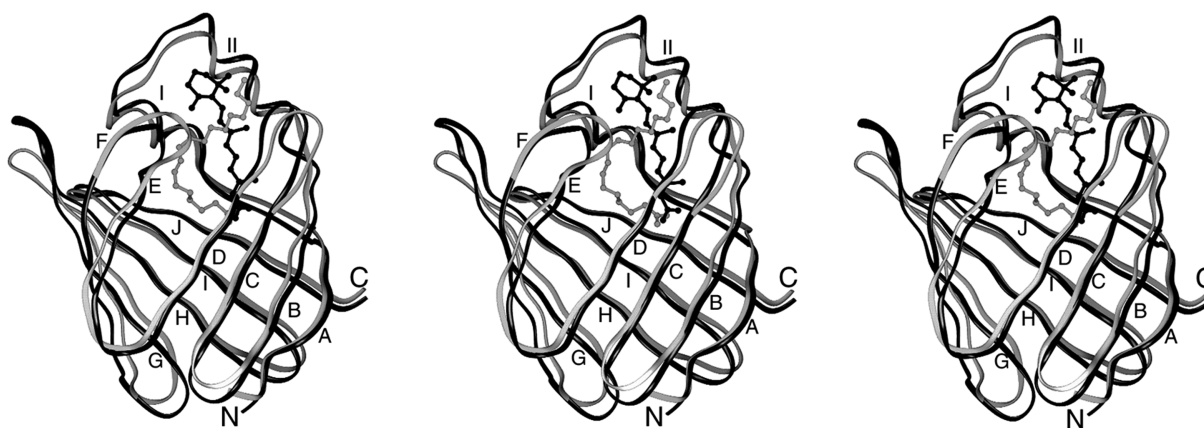


Fig. 2. Structural alignment of oleic acid (OA)-ALBP and retinoic acid (RA)-CRABP I. The left two images are in wall-eyed stereo, and the right two images are for use with cross-eyed stereo. The ALBP ribbon (1LIB) and corresponding OA ligand are in gray. CRABP I and RA (ICBP) are shown in black. β -strands are labeled with letters, and helices are labeled with Roman numerals. The beginnings and ends of the chains are marked with N and C, respectively. The figure was made with the computer program SETOR (58).

Because the cavity binding capacity exceeds the volume of the ligand, up to 20 water molecules must also be present. Some are visible in electron density maps, whereas others are disordered (3). NMR methods have also demonstrated special properties for a limited number of waters associated with these β -barrel proteins (4). In addition, the properties of the cavity waters have been modeled by a number of molecular dynamic studies (5–9). Because the ligands for this family are principally composed of methylene carbons ($-\text{CH}_2-$), the binding must include their interaction with water molecules within the cavity binding site.

In almost all of the crystallographic studies of the β -barrel proteins, some of the ligand atoms and nearly all of the water molecules have high-temperature factors. Furthermore, the electron density for lipid ligands is often not contiguous; therefore, as will be seen in Result, the overall conformation of the lipid ligand must be surmised from the electron density that is visible. In terms of crystallographic studies, although there may exist some doubt about the overall conformation of the bound lipid, its general location is unambiguous within the framework of the binding protein. As illustrated in Fig. 2, the retinoid is shifted within the cavity in relation to oleic acid (OA), and the experiments described below involve a selected triple mutation to determine if repositioning of the hydrophobic ligand for ALBP is obtainable.

The triple mutation described below involves one of the subtle conformational differences between apo- (indicating crystal structure without ligand bound) and holo-states in the $\beta\text{E}-\beta\text{F}$ loop region of CRABP I compared with ALBP. A summary of the differences in the crystallographic structures is as follows: 1) the side chain of I73 in ALBP is pointing away from the cavity, whereas the equivalent glutamic acid in CRABP I is involved in a hydrogen bond with R59 (2) (K58 in ALBP); 2) A75 in ALBP is close to the ligand in all known holo-structures, whereas the equivalent valine in CRABP I is swung into the cavity op-

posite the ligand; and β) the side chain of D77 in ALBP is pointing into the cavity, whereas the equivalent residue in CRABP I is a glycine. The result of these differences is that the entire β E- β F loop is pulled into the cavity of the holo-CRABP I structure compared with the apo-protein and the apo- and holo-ALBP structures. The triple mutation, E73I/A75V/D77G, of ALBP in principle mimics the entire β E- β F loop of CRABP I.

By way of further introduction, the structural data for many of these β -barrel proteins have been supplemented with extensive studies of the affinity and the underlying thermodynamics of lipid binding (10–12). ALBP binds fatty acids in the nanomolar to low micromolar range but binds RA less tightly (13). This can be compared with CRABP I, which binds RA in the nanomolar range but does not bind fatty acids with appreciable affinity (14). In general, the binding energy is mainly derived from enthalpic effects (15). However, in single-site mutants of the protein, less favorable enthalpic contributions are often compensated for by entropic changes (12).

MATERIALS AND METHODS

Chemicals used in protein expression, purification, and denaturation studies were from USB, Sigma, Mallinckrodt, Amer sham, Bio-Rad, PerSeptive Biosystems, Baker, and Fisher Biotech. Plasmids, cells, and standard reagents for plasmid DNA manipulations were obtained from Novagen, Clontech, BioLabs, Promega, Boehringer Mannheim (Roche), and Stratagene. Promega Wizard™ kits were used to clean some DNA fragments.

The triple mutation

The EF-ALBP mutation, I73E/A75V/D77G, was made by single-stranded site-directed mutagenesis (16) in the pJMB100A vector containing the murine ALBP gene (17). The triple mutation was introduced using the oligonucleotide primer with the sequence 5' GCT CTT CAC CTT CCT GCC GTC GAC GGT TTC TTC ATC GAA TTC CAC G 3'. Oligonucleotides for mutagenesis, PCR, and sequencing were synthesized at the Microchemical Facility at the University of Minnesota. The cDNA sequence was confirmed by the Microchemical Facility using the primer 5' GTC GAT AAG CTC TGC TGC AAC 3'.

For protein expression, the EF-ALBP cDNA was subcloned by PCR amplification using primers that introduced flanking *Bam*HI and *Nde*I restriction enzyme sites (primers: *Nde*I, 5' GGT TTA CCA TAT GTG TGA TGC CTT TG 3'; and *Bam*HI, 5' TTG ATG GAT CCT TCC ATC CAG GC 3'). PCR products were gel purified (low-melting-temperature SeaPlaque® agarose from FMC and GELase™ Agarose Gel-digesting Preparation from Epicentre Technologies), digested, and ligated into the pRSET vector (18, 19) at the *Bam*HI and *Nde*I sites. Sequencing was confirmed by the Microchemical Facility using pRSET sequencing primers for the T7 promoter and terminator sites (19).

Typically, 6 liters of EF-ALBP/pRSET or wild-type (WT)-ALBP/pRSET [media containing 16 g bactotryton, 5 g yeast extract, and 5 g NaCl per 1 liter (2 \times YT)] was induced with 0.4 mM isopropylthio- β -galactoside in *Escherichia coli* strains BL21(DE3) or BLR(DE3) when the optical density at 600 nm reached 0.4–0.6. Growth was then continued for 2.5–5 h. Cells were harvested by centrifugation at 4°C for 20 min at 3,100 *g* and were lysed either by sonication or by a modified method of freezing and thawing (20) in the presence of Complete™ protease inhibitor cock-

tail (Boehringer Mannheim, Roche) in 25 mM imidazole, pH 7.0, 50 mM NaCl, 5 mM EDTA, and 1 mM DTT buffer. When sonication was used, the buffer-cell paste ratio was 2:1 (v/w). For the freeze/thaw method, an equal volume of buffer was added to the cells in the final thawing stage and stirred for 30–60 min at 4°C. Soluble and insoluble fractions were separated by centrifugation at 4°C for 20 min at 5,000 *g*. Soluble and insoluble fractions were checked for the presence of recombinant protein by SDS-PAGE with Coomassie blue staining. CRABP I expression was done as previously described (21).

Purification and crystallization of EF-ALBP

The soluble extract from the EF- or WT-ALBP strains was treated with 10% polyethyleneimine (PEI) to a final concentration of 0.35% and centrifuged. The soluble fraction was then taken to pH 5.0 with 2 M NaAc, and the mixture was stirred overnight at 4°C as described by Xu et al. (22). The resulting precipitate was removed by centrifugation, and the soluble fraction was taken to 30% saturation with ammonium sulfate. The supernatant was concentrated to a final volume of 5–10 ml and fractionated on a Sephadex fine or superfine G-75 (5 \times 200 cm) or G-50 (5 \times 100 cm) gel filtration column using a pH 7.4 buffer (12.5 mM HEPES, 250 mM NaCl, and 1 mM DTT). If further purification was needed, it was achieved using a second gel filtration column (G-50, 2 \times 150 cm). Samples were delipidated with Lipidex1000 (hydroxyloxypropyl-dextran lipophilic-hydrophilic gel type VI; Sigma) in 20 mM potassium phosphate, 1 mM DTT, and 1 mM EDTA, pH 7.1, at 37°C to remove exogenous bound fatty acids (23, 24). CRABP I purification was done as previously described (21).

EF-ALBP protein at 9.0 mg/ml in 12.5 mM HEPES buffer, pH 7.2, was used for apo- and holo-crystallization trials using the hanging-drop/vapor diffusion (3 μ l of protein, 3 μ l of mother liquor) methods. Factorial NaH₂PO₄/K₂HPO₄ buffer (1.5 to 3 M, pH 5.8 to 7.8) (25, 26) and scans of 24–34% polyethylene glycol (PEG) 4K, 0.1–0.2 M NaAc, pH 7.4, and 0.1 M (NH₄)₂SO₄ crystal screening conditions were investigated (27). OA cocrystallization experiments were prepared with varying ligand-protein ratios and with fatty acids treated in different ways. These included protein-ligand ratios of 2:1 with sodium OA in 50:50 ethanol-water, 5:1 with sodium oleate in 100% ethanol, and 2:1 with sodium oleate in pH 12 water. Cocrystallization experiments were also prepared with ligand-protein ratios of 5:1 with RA in 100% ethanol and 5:1 with 1-anilino-naphthalene-8-sulfonic acid (ANS) solubilized in water.

X-ray data collection and structure determination

The X-ray data from crystals of apo-EF-ALBP were collected on a Siemens X-1000 multiwire area detector with CuK α radiation from a rotating-anode Rigaku RU-200 generator operating at 45 kV/200 mA with a graphite crystal monochromator. Data collection was carried out at room temperature at a detector distance of 110 mm with the crystal mounted in a capillary tube. Indexing, integration, scaling, and merging were handled with the XENGEN suite of programs (28). The apo-EF-ALBP structure was solved by using the coordinates of WT-ALBP (1LIB), having removed all water and ion molecules, alternative conformations, and changing the mutation sites (residues 73, 75, and 77) to alanines to calculate the first set of phases.

The OA-EF-ALBP crystal data set was collected with an R-AxisIV²⁺ image plate system at –160°C and a detector distance of 110 mm, with 2 θ = 0. The crystal was cryogenically protected with PEG 400 in short 5, 15, and 25% (v/v) soaks. Reflection indexing, integration, scaling, and merging were done with the program CrystalClear (29). The OA-EF-ALBP structure was solved by using the coordinates of apo-EF-ALBP at a refinement stage of Rfactor/Rfree being 0.18/0.22, having removed all water molecules, and alternative conformations to calculate the first set of phases.

Energy minimization refinement was implemented in cycles using X-PLOR (30) for apo-EF-ALBP and CNS (31) for OA-EF-ALBP. Electron density maps and model adjustments between refinement cycles were made and visualized in O (32), making use of both $2|F_o| - |F_c|$ and $|F_o| - |F_c|$ maps at varying contour levels. The DATAMAN program (33) was used to divide reflections into working and test sets. Rfactor/Rfree values were monitored throughout refinement (34). The addition of water molecules to the models had to fit standard X-ray crystallographic water criteria used in previous ALBP structures (17, 25, 26).

PROCHECK (35) was used to evaluate the quality of the final model. The CAST web server (<http://sunrise.cbs.umn.edu/cast/>) was used to analyze WT-ALBP and EF-ALBP protein pockets (cavities) and their openings as determined by molecular surface and accessible surface (36).

Chemical studies

The unfolding of apo-WT-ALBP and apo-EF-ALBP was measured by following the change in intrinsic tryptophan fluorescence in the presence of increasing amounts of guanidine hydrochloride (GdnHCl) or urea. Experiments were performed in 50 mM sodium phosphate buffer, pH 7.4, at 25°C with an ISS K-2 multifrequency phase fluorometer. Samples of 1 μ M apo-WT-ALBP or apo-EF-ALBP (0.5 to 3 ml) were preincubated for 2–4 h at room temperature with GdnHCl in 0.25 M increments from 0 to 3 M (4 M for apo-WT-ALBP) from a 6 M GdnHCl stock and urea in 0.5 M increments from 0 to 9 M from a 10 M urea stock. Measurements were made in triplicate. With the excitation wavelength set at 280 nm, emission profiles were scanned from 300 to 450 nm. The emission wavelength corresponding to the highest raw tryptophan fluorescence value for each scan was then plotted against the concentration of denaturant used at that point. The midpoints of unfolding were determined from the denaturation curves. Gibb's free energy was determined by the ratio of denatured to native protein at each concentration of denaturant and then extrapolation to the zero-point concentration (37, 38).

The ability of apo-EF-ALBP to bind ANS was measured and compared with apo-WT-ALBP and apo-CRABP I binding of ANS (ISS K-2 fluorometer). ANS solutions were prepared in water and the concentrations determined spectrophotometrically using $\epsilon = 4,990 \text{ l}\cdot\text{mol}^{-1}\cdot\text{cm}^{-1}$ at 350 nm in water (Fluka). Delipidated protein was titrated into 500 nM ANS in 50 mM phosphate buffer, pH 7.4, at 25°C. The excitation wavelength was set at 350 nm, and fluorescent enhancement upon protein addition followed over emission wavelength scans from 440 to 490 nm. The data for the displacement of ANS using OA and RA reported in Table 2 have not been corrected for inner filter effects (39, 40). Samples were stirred for 30 s before each reading. Measurements were made in triplicate. Absolute fluorescence data points at the maximum emission wavelength for each protein were plotted against increasing concentrations of protein. Raw fluorescence was scaled to put protein samples on the same scale. All work with ANS was done in low light, as ANS is light sensitive. A K_d^{ANS} was calculated for each titration using a variation of the equation derived by Kirk, Kurian, and Prendergast (39) and KaleidaGraph 3.5 Synergy Software (41) and subsequently averaged.

Displacement of bound ANS by OA and RA was measured for WT-ALBP and EF-ALBP (ISS K-2 fluorometer at 25°C). Under these conditions, CRABP I did not bind ANS tightly enough to be displaced with reliable measurements. This has been seen in previous studies as well (13). Sodium oleate (Sigma) was dissolved in water at pH 12. RA (Sigma) was dissolved in 100% ethanol. Five hundred nanomolar each of ANS and protein (WT-ALBP or EF-ALBP) was mixed in 50 mM sodium phosphate, pH 7.4. The excitation wavelength was set at 350 nm, and the quenching of bound ANS fluorescence was followed with emis-

sion scans from 440 to 490 nm. Samples were stirred for 30 s before each reading. Measurements were made in triplicate. Absolute raw fluorescence at the maximum emission wavelength for each protein was plotted against increasing concentrations of OA or RA. Raw fluorescence was then adjusted to put each run on the same scale. The ligand concentration at the midpoint of displacement was calculated and entered into the displacement equation from Simpson and Bernlohr (13, 42, 43). K_d values were calculated for each displacement and averaged. RA titrations were not corrected for inner filter effects (39, 40).

The thermodynamic parameters of OA binding to EF-ALBP and WT-ALBP were studied using an isothermal titration calorimeter (ITC Microcal OMEGA system). Sodium oleate (1.2 mM) was prepared in 20 mM potassium phosphate, 50 mM KCl buffer, pH 7.2, and was titrated into 2 ml of protein solution in 30–40 separate 3–7 μ l injections at 25°C. Protein concentrations were typically 48 μ M WT-ALBP and 58 μ M EF-ALBP. Titrations were done in triplicate, and buffer was titrated into protein alone. We were unable to find a suitable solvent to prepare the RA that was not accompanied by large heats of dilution. Data were corrected for heats of dilution of OA, normalized, and interpreted using a nonlinear least-squares algorithm from the ORIGIN software package (44), accommodating three parameters: the association binding constant (K_a), the number of bound sites (n), and the enthalpy of binding (ΔH). The parameters K_d , ΔG , $-T\Delta S$, and ΔS were then calculated from the n , K_a , and ΔH values estimated by the curve-fitting procedure. Each calorimeter run was analyzed separately, and the results were averaged for each protein.

RESULTS

The isolated protein was characterized by SDS-PAGE and was judged to be homogeneous after two gel filtration steps. Crystallization conditions for the apo-EF-ALBP included 2.1 M $\text{NaH}_2\text{PO}_4/\text{K}_2\text{HPO}_4$ buffer, pH 7.0. Slightly different conditions were found for the protein/fatty acid complex, for which the best crystals were obtained from solutions containing 2.7 M $\text{NaH}_2\text{PO}_4/\text{K}_2\text{HPO}_4$ buffer, pH 6.8, and a protein-ligand ratio of 2:1, with the sodium oleate in a 1:1 water-ethanol solution. A model of the apo-EF-ALBP structure was obtained using the WT-ALBP coordinates (1LIB), followed by rigid body (45), positional minimization, and a series of simulated annealing refinement protocols (46). Refinement included the use of bulk solvent corrections (47) and intermediate empirical calculations to adjust the weighting of X-ray versus canonical contributions.

The X-ray data collection statistics and properties of the crystallographic models are given in Table 1. The low value of R_{merge} and the final correspondence between the observed and calculated structure factors suggest reliable coordinates for both crystallographic studies. After minimization and individual B-factor refinement, electron density at the sites of the residue changes was clearly visible and modifications were made to include the correct atoms. The correspondence between the amino acid mutations and the final electron density is visible in Fig. 3.

Even though several unique X-ray data sets were collected, electron density observed in the cavity of the OA-EF-ALBP structure continued to be difficult to interpret (Fig. 4) and a number of structures were refined. The first fatty acid conformation was taken from the OA-WT-ALBP struc-

TABLE 1. EF-ALBP X-ray data and refinement statistics

Parameter	Apo-EF-ALBP	OA-EF-ALBP
Cell parameters (Å)	120.1, 38.0, 28.8	118.9, 36.9, 27.9
(°)	$\alpha = \gamma = 90, \beta = 92.3$	$\alpha = \gamma = 90, \beta = 92.6$
Space group	C2	C2
Resolution (Å)	8–1.5	25–1.7
Total observations	83,041	42,285
Unique reflections	31,800	13,235
Redundancy	2.61	3.19
Average I/ σ I	34.6	16.4
Completeness (%)	89.0	93.9
R _{merge} (%)	4.5	4.6
R _{factor} /R _{free} (%)	19.6/22.5	20.8/23.7
Protein atoms ^a	1123	1087
Mean protein atom B factor (Å ²)	14.5	23.1
Ligand atoms ^b	0	40
Mean ligand atom B factor (Å ²)	0	35.6
Water molecules	84	120
Mean water molecule B factor (Å ²)	25.0	32.8
Ion atoms	5	5
Mean ion atom B factor (Å ²)	36.7	35.2
RMSD bond lengths (Å)	0.006	0.008
RMSD bond angles (°)	1.3	1.4
Protein Data Bank accession code	1G7N	1G74

R_{merge} denotes the normalized percent error between equivalent Bragg reflections measured multiple times; it is an estimate of the quality of the X-ray diffraction data. R_{factor}/R_{free} indicates the relative agreement between the calculated and observed structure factors for each of the models deposited in the PDB. R_{free} is calculated from X-ray data not included in the model refinement and should approach R_{factor} as the refinement converges.

ALBP, adipocyte lipid binding protein; apo-, crystal structure without ligand bound; OA, oleic acid; RMSD, root mean square distance.

^aProtein atoms include alternative conformations.

^bLigand atoms for the OA-EF-ALBP complex include two conformations for the ligand, each modeled at 50% occupancy. The Protein Data Bank coordinates have been deposited.

ture (1, 48), but it overlapped with the position of a side chain, F57. A second unsatisfactory interpretation was made based on the conformation of arachidonic acid bound to WT-ALBP (26). A third interpretation was based on two fatty acid conformations with partial occupancy, with head groups modeled after the OA position in OA-WT-ALBP and the RA position in RA-WT-CRABP I. The methylene atoms were modeled along opposite sides of the cavity. However, these results were not satisfactory, as negative electron density peaks resulted over the placed ligand head groups.

Finally, two U-shaped conformations of OA, differing from each other by a rotation of almost 180°, were used in-

dependently in separate refinement protocols. In neither orientation was there electron density for C₁₈ of the OA, and the positioning of the carboxylate head group was uncertain but clearly different from that described for WT-ALBP (1). With no distinguishable electron density for the carboxylate(s), the final stages of refinement were done using both fatty acid conformers each at 50% occupancy. The coordinates for apo-EF-ALBP and OA-EF-ALBP (with both OA conformations at 50% occupancy) have been deposited in the PDB with accession numbers 1G7N and 1G74, respectively. The duplicity of fatty acid conformers will be described in more detail in the Discussion section.

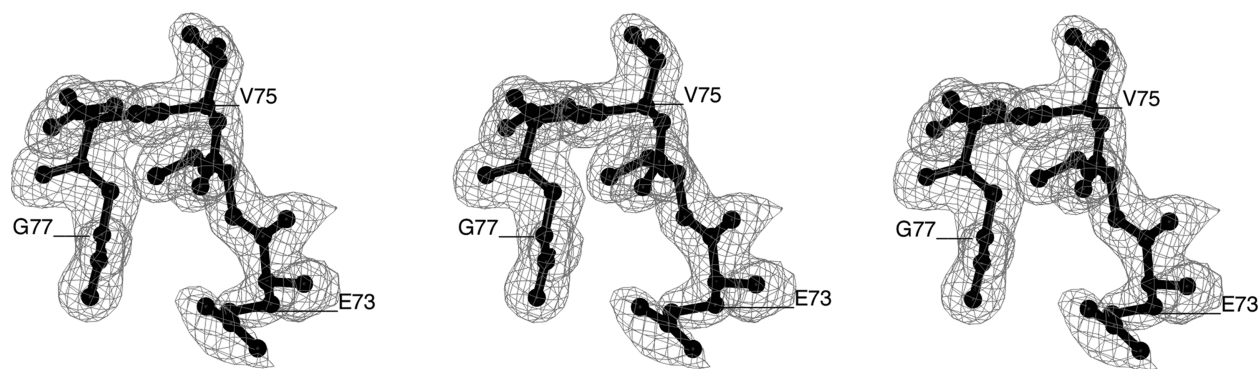


Fig. 3. Electron density for the EF-ALBP mutation site. The left two images are in wall-eyed stereo, and the right two images are for use with cross-eyed stereo. The crystallographic structure of the β E- β F loop is shown. The $2|F_o| - |F_c|$ density at 1σ contouring clearly shows the correct mutations at I73E, A75V, and D77G. Labels mark the C α atoms, with the main chain extending before and after residues E73 and G77. The drawing was made with the computer program SPOCK (59).

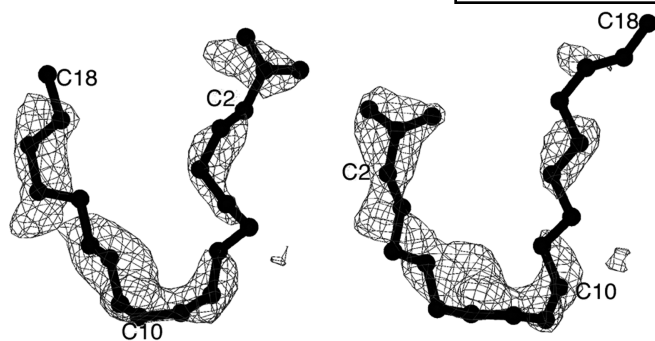


Fig. 4. OA in the crystal structure of the holo-form of EF-ALBP. This illustration depicts the electron density for two OA positions in crystalline EF-ALBP. Electron density is contoured at 0.8σ ($2|F_o| - |F_c|$). Final rounds of refinement were performed on each model separately and therefore resulted in a unique phase set and electron density map. Interactions of the two OA positions with EF-ALBP are listed in **Table 4**.

Protein stability

The duplicity of OA positioning in EF-ALBP, compared with WT-ALBP, suggested that other differences should be observable in the mutant protein, including its overall stability and some of the lipid binding properties. Surprisingly, EF-ALBP proved to be slightly more stable than WT-ALBP, as determined by shifts in the maxima of fluorescence intensity in denaturation profiles (supplemental data, Fig. 1S). The denaturant concentrations at the unfolding midpoint increased by 19% in urea and 12% in Gdn-HCl. When the unfolding curves are analyzed in terms of the apparent Gibbs free energy of unfolding (ΔG_{app}°), EF-ALBP is more stable by a factor of $\sim 20\%$. The ΔG_{app}° values for WT-ALBP and EF-ALBP were calculated as 2.05 and 2.59 kcal/mol in urea and 3.09 and 3.75 kcal/mol in Gdn-HCl, respectively. Altering the side chains at the turn between βE and βF resulted in an increase in protein stability.

Ligand binding and displacement

A dramatic enhancement in fluorescence occurs when ANS binds to members of the family of lipid binding proteins, including ALBP and CRABP I. As a result, the ANS binding reaction has been used successfully to study the binding cavities of ALBP and other family members (13, 39, 49). The displacement of ANS from the protein by other ligands may also provide some measure of their affinity. These properties of ANS are particularly useful because other ligands, such as fatty acids and retinoids, are not very soluble in aqueous buffers and at high concentrations form a second micellar phase. Hence, ANS binding was used to obtain some idea about changes in the lipid binding properties of EF-ALBP. The limited results given below represent studies of changes within the cavity that have occurred as a result of the triple mutation.

The K_d^{ANS} values for ANS binding to WT-ALBP, EF-ALBP, and CRABP I, and the K_i values for OA and RA displacement of bound ANS, are reported in **Table 2** (Figs. 2S and 3S in the supplemental data contain the experimental results used to prepare Table 2). The K_d^{ANS} values show that ANS binds to

WT-ALBP and EF-ALBP with nearly equal affinity and that CRABP I binds ANS considerably less tightly. Differences between the K_d^{ANS} values for WT-ALBP and EF-ALBP are not significant, as demonstrated by the P value (Table 2). The K_i values in Table 2 suggest that compared with WT-ALBP, EF-ALBP mutant binds OA and RA with similar affinity. Differences between the K_i^{OA} values for WT-ALBP and EF-ALBP are not significant (Table 2). The K_i^{RA} values for WT-ALBP and EF-ALBP initially appear to indicate that the mutant binds RA slightly less tightly, but calculated P values support the notion that the changes are not statistically significant (Table 2). The K_d for ANS binding to CRABP I was found to be $26,400 \pm 6,140$ nM, agreeing well with results from other workers (25,000 nM) (13). Previous literature for WT-ALBP (undelipidated) reports slightly less affinity for ANS binding (410 nM), similar displacement by OA (130 nM), and RA displacement values (870 nM) suggesting weaker RA binding than reported here (13). The data reported here were derived from delipidated samples (see Materials and Methods), as opposed to the undelipidated sample values reported in the literature, and could play a role in the increased binding values observed in this study. Using the ANS displacement results, the triple mutation appears to have not significantly changed the affinity of ALBP for OA or RA.

To probe further into the lipid binding properties of the mutant, isothermal titration calorimetry was used to evaluate OA binding. This experiment provided both the enthalpic and entropic components of the binding reaction, and the results are summarized in **Table 3** (typical experimental results are shown in Fig. 4S in the supplemental data). During the numerical determination of K_d , attempts were made to set $n = 1$. The free energies of binding OA to both WT-ALBP and EF-ALBP were relatively similar. However, statistically significant differences were found between the enthalpic and entropic components. The EF-ALBP value for the enthalpic component (ΔH^0) value is positive, whereas the WT-ALBP value is negative. The ΔS^0 for the EF-ALBP mutant is positive and larger than that for WT-ALBP. Values for n for both WT-ALBP and EF-ALBP deviated from the expected values of 1.

DISCUSSION

The crystallographic studies and the duplicity of positioning OA in crystalline EF-ALBP, along with the comparison of ligand positioning in the various holo-forms of

TABLE 2. ANS binding and displacement for WT-ALBP, EF-ALBP, and CRABP I

Parameter	WT-ALBP	EF-ALBP	P^a	CRABP I
K_d^{ANS} (nM)	170 ± 20	300 ± 190	0.3039	$26,200 \pm 6,140$
K_i^{OA} (nM)	190 ± 70	290 ± 60	0.1335	ND
K_i^{RA} (nM)	380 ± 180	930 ± 370	0.0816	ND

Data are expressed as means \pm SD. ANS, 1-anilinonaphthalene-8-sulfonic acid; CRABP I, cellular retinoic acid binding protein type I; ND, not determined; RA, retinoic acid; WT, wild-type.

^a P values are shown for unpaired t -test analysis of EF-ALBP and WT-ALBP values. $P < 0.05$ is considered statistically significant.

TABLE 3. Isothermal titration calorimetry analysis for WT-ALBP and EF-ALBP

Parameter	WT-ALBP (OA)	EF-ALBP (OA)	$\Delta\Delta^a$	p^b
K_d (μM)	1.8 ± 0.7	0.30 ± 0.2	0.0234	
n (ligands)	0.7 ± 0.2	1.4 ± 0.1	NA	
ΔG (cal/mol)	$-7,860 \pm 240$	$-8,940 \pm 330$	+1,080	0.0102
ΔH (cal/mol)	$-1,080 \pm 80$	$1,120 \pm 100$	-2,200	0.0001
ΔS (cal/deg/mol)	22.8 ± 2.3	33.8 ± 1.2	-11.00	0.0018

Data are expressed as means \pm SD. NA, not applicable.

^a $\Delta\Delta$ values were calculated by subtracting EF-ALBP values from WT-ALBP values. The experimental results are the average of three independent experiments.

^b P values are shown for unpaired t -test analysis of EF-ALBP and WT-ALBP values.

ALBP and the location of RA in CRABP I, suggest that more than the protein atoms define the stereochemical nature of the ligand interactions. It was the appearance of discrete disorder found in the electron density of crystalline EF-ALBP with OA that drew our attention to the limiting volume available to the bound lipids. As will be demonstrated below, although the surface contour of the binding site is irregular, it appears that the ligands tend to locate only within a narrow planar region in the ALBP cavity. In addition, the rudimentary binding studies described in Results provide evidence for changes in ligand affinity as a result of the triple mutation. Although the chemical studies are incomplete regarding the change to RA specificity, they do provide evidence for changes in the protein-ligand interactions in the solution state.

Chemical changes in EF-ALBP

The triple mutation present in EF-ALBP resulted in a slightly more stable protein than its WT predecessor. The

TABLE 4. OA-WT-ALBP and OA-EF-ALBP protein-ligand contacts

Residue	WT-ALBP	OA-EF-ALBP (A)	OA-EF-ALBP (B)
Contact by van der Waals radii			
F16		X	X
Y19			X
M20	X	X	
V25		X	
T29	X		
V32	X		
A33	X		X
A36		X	
P38		X	X
M40		X	X
S55			X
F57	X		X
K58	X		
A75	X		X
D76	X	X	
I104			X
V115		X	X
C117	X	X	X
R126		X	X
Y128			X
Contact by H-bonds			
S55			X
R126	X		
Y128	X		

Contacts were calculated by LIGPLOT (60).

increased stability was demonstrated by both urea and guanidine denaturation studies. Although it is not possible to correlate the observed changes with any long-range interactions, the crystal structures of the wild type and the mutant were reexamined to determine if there were any discernible short-range interactions that would explain this modification. A summary of short-range changes is as follows. The A75V alteration adds a larger hydrophobic residue that provides a potential nonpolar interaction with the bound fatty acid. But this does not explain the improved stability of the apo-form. The I73E change could possibly be a stabilizing feature, because this residue is located on the surface near the midway point between two lysine side chains: K58 and K79. More favorable electrostatic energy is likely based on simple coulombic interactions. The replacement of D77 with a glycine may contribute to the stability, as it is located in a relatively tight turn where a side chain might be destabilizing (50). Viewed in a qualitative manner with insight only to short-range effects, all three changes might contribute to the improved stability, but again, this speculation ignores the long-range changes that might have occurred.

Because both binding and crystallographic data are available on ANS binding to ALBP (13, 42, 49), the EF-ALBP changes were examined using this fluorescent probe. The K_d^{ANS} values presented in Table 2 indicated that the new EF-loop had little effect on ANS affinity. Using the superimposed model coordinates, the positioning of the ANS within the binding site was compared with that of the fatty acids and RA. The overlaid structures shown in stereo in Fig. 5, top and bottom panels, indicate that ANS (deep blue molecule) binds at a position overlapping both the RA site in CRABP I and the fatty acid site in ALBP.

Studies of ANS binding were extended to include its displacement from the binding cavity by OA and RA. The resulting K_i is an indirect measurement of the binding affinity of other ligands, and the values for OA and RA are given in Table 2. From these values, EF-ALBP appeared to bind both ligands with similar values as those found for WT-ALBP. From the crystallographic studies described above, the binding of OA to EF-ALBP is substantially different from that of the native protein (Fig. 5, top and bottom panels, brown molecules). The relative similarity in binding affinity of both proteins for OA might suggest that the mutations in this one loop of the β -barrel had little effect on the thermodynamic properties. This was not the case.

The thermodynamic components of OA binding to EF-ALBP as determined by isothermal titration calorimetry studies are considerably different from those of WT-ALBP. The results are shown in Table 3 and suggest that the mutation may cause significant changes in the components of protein-ligand interactions. Literature values for WT-ALBP and OA list $K_d = 2.4 \pm 1.0 \mu\text{M}$, $n = 0.9 \pm 0.2 \text{ mol/mol}$, $\Delta G = -7,770 \pm 580 \text{ cal/mol}$, $\Delta H = -6,050 \pm 1,320 \text{ cal/mol}$, and $T\Delta S = 1,720 \pm 1,340 \text{ cal/mol/K}$ (26). These values differ slightly from those reported here but were collected under different chemical conditions. With positive ΔH values and a large ΔS , the binding reaction for the mutant protein is entropically driven and endo-

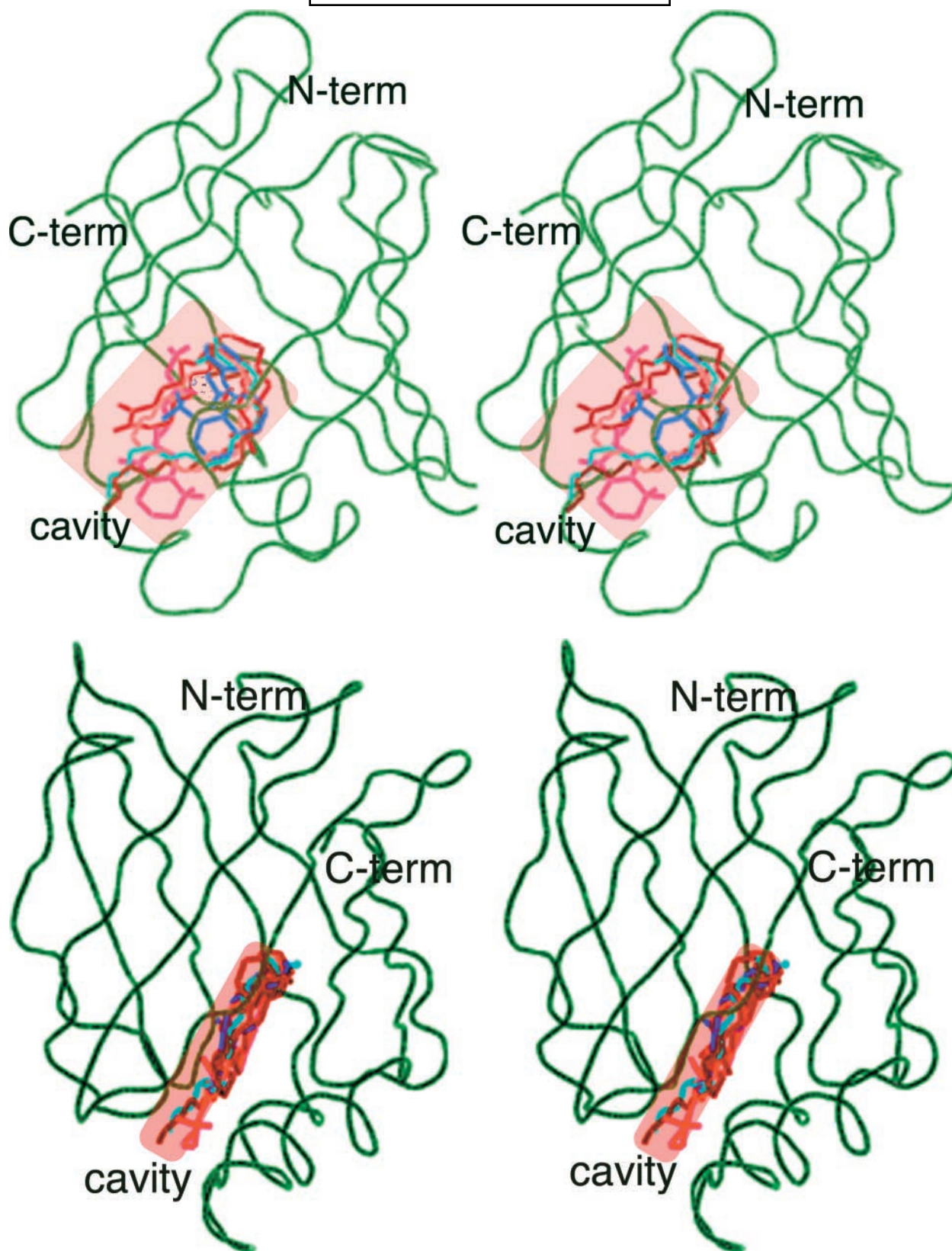


Fig. 5. Lipid ligands in β -barrel proteins. Top and bottom panels: Stereo drawings with the main chain illustrated as a ribbon in green. These drawings differ only by the viewing angle: in the top panel, the viewer is looking perpendicular to the ligand binding plane, and in the bottom panel, the view is edge on. The different lipids are color-coded as follows: brown, the static disordered oleates in EF-ALBP; red, RA from CRABPI as described in the text; blue, 1-anilinoanthracene-8-sulfonic acid as found in ALBP; cyan, arachidonate in ALBP; pink, OA in ALBP.

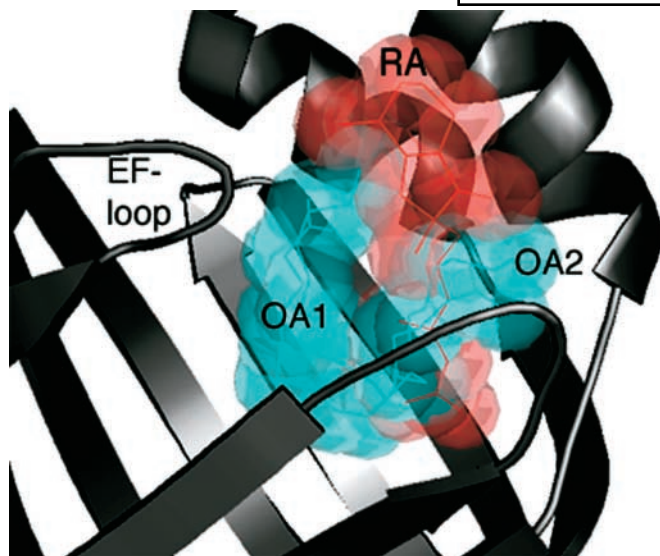


Fig. 6. Cartoon drawing of EF-ALBP in gray with the two positions of OA in EF-ALBP drawn with blue and partially transparent spheres. The alternative fatty acid sites are labeled OA1 and OA2. Again with van der Waals spheres, RA in CRABP I is shown in red. The overlap between RA and OA2 is visible to the right of the plane. The position of the triple mutation is labeled EF-loop.

thermic, whereas for the WT-ALBP protein, it is enthalpically driven and exothermic. Generally, most enthalpic contributions arise from the balance of noncovalent bonding, such as various polar interactions. The burial of nonpolar residues, solvent reorganization, and significant structural changes have been associated more with systems of entropic character (51–53).

In view of the crystallographic results on holo-EF-ALBP, the repositioning of the carboxylate belonging to the ligand may account for changes in the enthalpic component. In ALBP, the carboxylate of the fatty acid interacts with polar side chains, including two arginines and a tyrosine. This head group position would correspond to the location of the anionic group of OA, hexadecane sulfonic acid, and arachidonic acid shown in Fig. 5, top and bottom panels. The X-ray crystallographic studies of EF-ALBP left uncertain the positioning of the carboxylate (Fig. 4). The head groups were initially refined into the broadened segments of electron density shown in Fig. 4, each appearing when one of the two conformers was refined without the other. In the final X-ray interpretation, they were modeled with discrete disorder in two conformations. In both locations, the carboxylates were not located in the same position as they were in the WT protein. Although somewhat ambiguous, the final crystallographic structure included both duplicity in the hydrocarbon chain orientation and a positioning of the carboxylates different from that assigned in the WT crystalline ALBP.

With weaker polar interactions between the carboxylate head group of the OA and the protein, the binding reaction should be less enthalpically driven than when present in the binding site of WT-ALBP. Finally, it should be noted that similar thermodynamic changes were observed in

mutant forms of both ALBP and its intestinal homolog (12). In binding studies of many mutants of the β -barrel lipid binding proteins, Kleinfeld and coworkers (12) observed compensatory entropic and enthalpic changes. Although the basis of changes in the driving energies may not be explainable by the conformational data described in this report, it is clear that the triple mutation had a distinct effect on the cavity binding site.

Comparison of the crystal structures

To visualize the common regions occupied by ligands in different crystal structures, overlays were made by the method of least squares using only the $C\alpha$ coordinates. The crystal coordinates of the holo-form of EF-ALBP were in close agreement with those containing other ligands, including arachidonic acid, ANS, oleate, decahexane sulfonic acid, palmitate, and RA (PDB accession codes 1ADL, 2ANS, 1LID, 1LIC, 1LIE, and 1CBQ, respectively). The mean of the standard deviations for the combined pairwise least squares overlays of the $C\alpha$ values was 0.4 Å.

With all of the coordinates of the holo-forms in the same frame, the positioning of the respective ligands could be compared within a single conformation of the protein, and the results were unexpected. As seen in Fig. 5 (top and bottom panels), one of the bound oleates (brown) overlays the structure of the same fatty acid in the WT protein (1), whereas the other appears where the RA is found in CRABP I (2). Bound ANS, aside from the sulfonic acid moiety, lies in the position of OA in the WT protein (49). The unexpected consequence of these calculations is the fact that the atoms that constitute all of the ligands lie close to being arranged in a single plane.

In the coordinate frame of the holo-form of EF-ALBP, the least-squares ligand plane is given by the equation $Ax + By + Cz = D$ and has the values of $A = -0.6786$, $B = -0.3633$, $C = 0.6384$, and $D = 1.905$. The root mean square (RMS) distance of all 145 carbon atoms of bound ligands to the least-squares plane is 0.734 Å. This RMS variation is close to the expected error in the coordinates, so the significance of the planar nature of the ligands is very noteworthy. During the review of this study, a referee noted that the fatty acids bound to the brain form of crystalline brain fatty acid binding protein (B-FABP) did not correspond to a planar conformation, and it is worth mentioning that not all family members have been compared in this report. In B-FABP, the end of the hydrocarbon chains (C16–C22 for docosahexaenoic acid and C16–C18 for OA) begin to form a helical conformation, and these carbons do not quite conform to a planar orientation (54).

The conformational basis of the planar nature of the acceptance site in the ALBPs and CRABP I is uncertain. The lipid binding sites in the β -barrel proteins are located in a cavity larger than most of the common methylene chains of the various ligands. With flexible ligands such as fatty acids, a reasonable expectation would be that the methylene carbons of a bendable ligand would lie along the walls of the cavity, following a set of nonplanar, nonpolar protein side chains or atoms. Instead, they are accommodated within a single plane as described above. One could

argue that it is water molecules within the cavity that are responsible for the planar limitations. This hypothesis will be difficult to prove, because the positioning of water sites in electron density is not always reliable. Whatever the explanation, if in fact ligand atoms may be placed within the cavity in a variety of planar positions, the entropic element to the binding stability is enhanced by allowing two degrees of motional freedom.

The crystal structures were also studied in the region of β E and β F strands. The location of the EF-loop was essentially unchanged by the triple mutation, but it produced observable chemical and structural changes within the cavity. The overlap between the RA binding site in CRABP I and the discrete disorder found in the fatty acids bound to EF-ALBP suggests that the changes were in the direction of the original design. This atomic coincidence between the location of RA compared with the two sites for OA is depicted in Fig. 6. The RA site in the β -barrel proteins is shown in red mesh, and the dual OA sites are shown as blue spheres. The right-most fatty acid site in Fig. 6 in EF-ALBP overlaps nearly in total the RA site in CRABP I. Furthermore, in CRABP I, movement of this EF-loop to the right would interfere with the left-most OA but not with the RA position.

Overall, major steric overlaps are visible between RA and one of the oleates bound to the crystalline form of the mutant. The overlap is particularly striking for the RA and the OA labeled OA2 in Fig. 6. Also visible in Fig. 6 is

the location of the EF-loop that contained the mutations. Although slightly off to one side, the tip of this loop points directly to the largest surface of the ligand binding box. Unfortunately, and contrary to the original expectations, no change in the positioning of the EF-loop was visible in either the electron density of the holo- or apo-crystal structures of EF-ALBP.

Comparison of apo- and holo-crystal structures

During the comparisons of the crystal structures in the region of the mutations, detailed overlays of apo- and holo-structures, of both mutant and wild type, were done. The general arrangement of secondary structural elements is very similar, but subtle differences in the positions of some side chains were apparent. These similarities apply to EF-ALBP both with and without bound OA. Several of the largest differences around P38 and K58 parallel those found between apo-WT-ALBP and OA-WT-ALBP. P38 is at the termination of the helix-turn-helix lid of the β -barrel, and carbon atoms belonging to its side chain point into the ligand binding cavity.

There were greater differences between the apo-EF-ALBP and OA-EF-ALBP structures near protein segments consisting of residues 44–46, 89–91, 107–113, and 121–122 compared with WT conformations. In contrast, the region around residues 73–77 (β E- β F turn) was not as different as that observed in the CRABP I versus ALBP WT conformations. All of these conformational differences

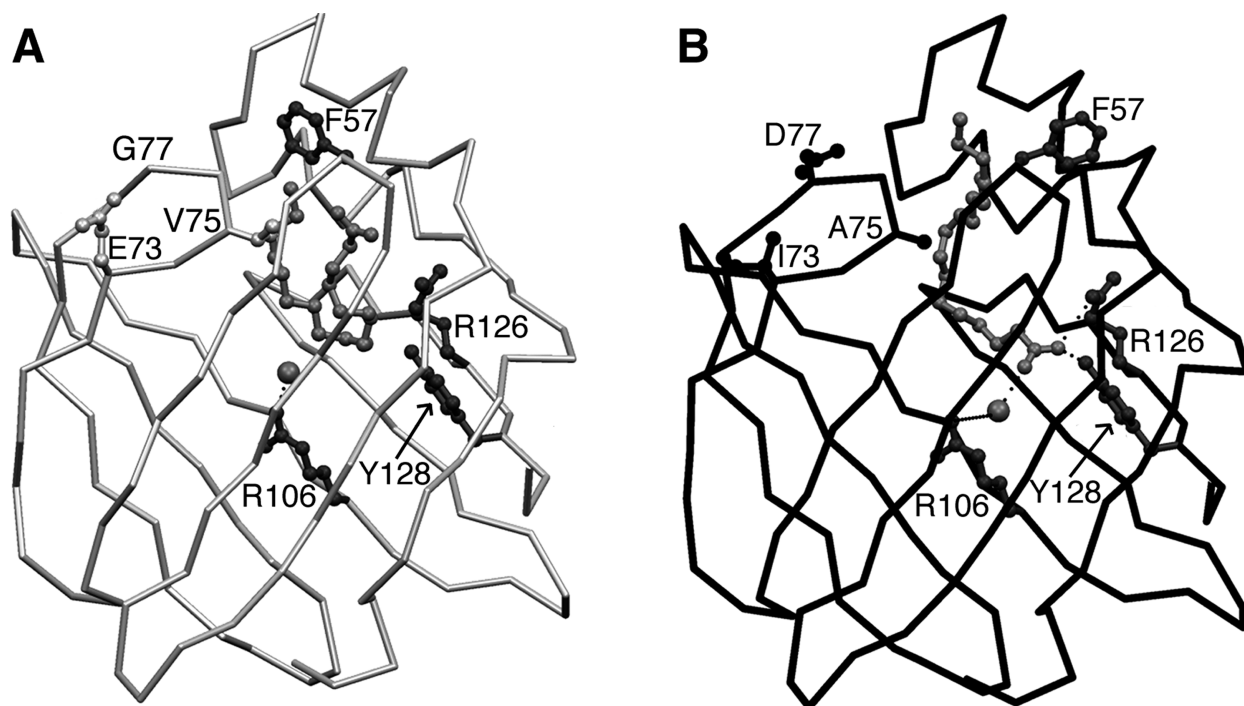



Fig. 7. EF-ALBP cavity relative to the WT-ALBP cavity. A: OA-EF-ALBP α chain and mutation sites are shown in light gray. B: OA-WT-ALBP α chain and equivalent WT residues are shown in black. OA is shown in medium gray in both panels. Cavity residues F57, R106, R126, and Y128 are shown in dark gray in both panels. A medium gray water molecule and its hydrogen bonding pattern are also depicted in each panel. In the case of OA-WT-ALBP in B, F57 is swung out of the cavity to make room for the ligand, which is then coordinated by the water molecule to R106. This does not happen in OA-EF-ALBP, as shown in A. The F57 does not move, and the water molecule is in a different position, unable to coordinate the carboxylate of the ligand in the usual conformation. The drawing was made with SETOR (58).

occur at secondary elements described as β -turns, and each includes a glycine residue. Although all of these differences are relatively small, overall the differences suggest that interconnecting turns of the β -barrel, along with the included glycines, may play a major role in the adjustment of these proteins to different lipids.

Some of the same side chains involved in the small conformational changes at interconnecting turns also have an effect on the internal cavity. Cavity accessibility measurements from the CAST program (36) indicate that residues around N45 and L91 in the apo-EF-ALBP and around A90 and K107 in the OA-EF-ALBP structure have increased accessible surfaces within the cavity. As with the other members of the protein family, the main binding cavity of the OA-EF-ALBP form (calculated without ligand present) is slightly larger than that for the apo-form (55).

Although no gross changes have occurred as a result of the triple mutation, some conformational differences are visible. The side chain of F57 in the OA-EF-ALBP structure (Fig. 7A) is not moved toward solvent to accommodate OA, as it apparently favors in the OA-WT-ALBP structure (Fig. 7B). Instead, it is found in good density pointing into the cavity, much like it is in the crystal conformation of apo-WT-ALBP. There is also a very important difference in the cavity water network between WT-ALBP and EF-ALBP. In WT-ALBP, there is a water molecule in the apo-structure that moves into place in the OA structure to coordinate with R106 (Fig. 7B). In the EF-ALBP crystal structures, the water locations are reversed between the apo- and holo-structures. This means that the water molecule is no longer available for coordinating to R106 and may explain why the commonly observed interaction between the carboxylate head group is not observed in OA-EF-ALBP. In turn, the lack of a carboxylate head group could theoretically explain the loss of the water molecule at that position.

In summary, the mutational studies were done to modify the ligand binding specificity of a β -barrel lipid binding protein. A variety of changes were observed, including the static disorder of fatty acid positioning. In the process of overlaying the ligands studied in a variety of crystal structures, the cavity binding site appears to be used in a planar manner in ALBP; that is, all of the nonpolar atoms observed in a collection of crystal structures lie in a relatively well-defined plane. Although the electron density for ligand atoms in these β -barrel proteins always appears weak, observable density appears to converge to a single plane. The planar conformations are observed even when a hydrocarbon chain has an overall U-shaped structure. The water network generates a sidedness to the planar binding aperture, but the range of binding positions within this planar site is uncertain. The triple mutation has clearly set up an alteration within the binding plane, and the crystallographic results demonstrate that one ligand segment now more closely resembles the positioning of RA in CRABP I. 

The authors thank the members of the Bernlohr laboratory for gifts of plasmids and cells and for molecular biology advice.

The authors also thank Bob Ledford for his assistance in initial EF-ALBP mutant protein expression, Judy Bratt for the purification of WT-ALBP and CRABP I, and Ed Hoeffner for his upkeep of the X-ray equipment. The authors appreciate the use of the fluorometer from the laboratory of Dr. David Thomas (University of Minnesota) and Dr. Greg Hunter's technical assistance. The authors are grateful for constructive conversations with members of both the Banaszak and Ohlendorf laboratories throughout the project. The resources of the Minnesota Supercomputer Institute (MSI) were used for model building and refinement, and Dr. Shuxia Zhang of the MSI wrote code to determine the properties of planes. Finally, the authors thank Dr. Melanie Simpson (University of Nebraska) and Dr. Eva Istavan (Washington University School of Medicine) for their insight during the preparation of the manuscript. This research project was supported by Grant GM-13925 (L.J.B.) and predoctoral Grant GM-08277 (A.J.R.) from the National Institutes of Health.

REFERENCES

1. Xu, Z., D. A. Bernlohr, and L. J. Banaszak. 1993. The adipocyte lipid-binding protein at 1.6-Å resolution. Crystal structures of the apoprotein and with bound saturated and unsaturated fatty acids. *J. Biol. Chem.* **268**: 7874–7884.
2. Kleywegt, G. J., T. Bergors, H. Senn, P. Le Motte, B. Gsell, K. Shudo, and T. A. Jones. 1994. Crystal structures of cellular retinoic acid binding proteins I and II in complex with all-trans-retinoic acid and a synthetic retinoid. *Structure*. **2**: 1241–1258.
3. Banaszak, L., N. Winter, X. Xu, D. A. Bernlohr, S. Cowan, and A. T. Jones. 1994. Lipid-binding proteins: a family of fatty acid and retinoid transport proteins. *Adv. Protein Chem.* **45**: 89–151.
4. Lucke, C., S. Huang, M. Rademacher, and H. Ruterjans. 2002. New insights into intracellular lipid binding proteins: the role of buried water. *Protein Sci.* **11**: 2382–2392.
5. Woolf, T. B. 1997. Molecular dynamics of individual α -helices of bacteriorhodopsin in dimyristyl phosphatidylcholine. I. Structure and dynamics. *Biophys. J.* **73**: 2376–2392.
6. Lucke, C., D. Fushman, C. Ludwig, J. A. Hamilton, J. C. Sacchetti, and H. Ruterjans. 1997. A comparative study of the backbone dynamics of two closely related lipid binding proteins: bovine heart fatty acid binding protein and porcine ileal fatty acid binding protein. *Third Int. Conf. Lipid-Binding Proteins*. **14**: 1–16.
7. Likic, V. A., and F. G. Prendergast. 2001. Dynamics of internal water in fatty acid binding protein: computer simulations and comparison with experiments. *Proteins*. **43**: 65–72.
8. Krishnan, V. V. 2000. Dynamics of cellular retinoic acid binding protein I on multiple time scales with implications for ligand binding. *Biochemistry*. **39**: 19–29.
9. Constantine, K. L., M. S. Friedrichs, M. Wittekind, H. Jamil, C. H. Chu, R. A. Parker, V. Goldfarb, L. Mueller, and B. T. Farmer II. 1998. Backbone and side chain dynamics of uncomplexed human adipocyte and muscle fatty acid-binding proteins. *Biochemistry*. **37**: 7965–7980.
10. Richieri, G. V., P. J. Low, R. T. Ogata, and A. M. Kleinfeld. 1997. Mutants of rat intestinal fatty acid-binding protein illustrate the critical role played by enthalpy-entropy compensation in ligand binding. *J. Biol. Chem.* **272**: 16737–16740.
11. Richieri, G. V., R. T. Ogata, and A. M. Kleinfeld. 1996. Thermodynamic and kinetic properties of fatty acid interactions with rat liver fatty acid-binding protein. *J. Biol. Chem.* **271**: 31068–31074.
12. Richieri, G. V., P. J. Low, R. T. Ogata, and A. M. Kleinfeld. 1998. Thermodynamics of fatty acid binding to engineered mutants of the adipocyte and intestinal fatty acid-binding proteins. *J. Biol. Chem.* **273**: 7397–7405.
13. Kane, C. D., and D. A. Bernlohr. 1996. A simple assay for intracellular lipid-binding proteins using displacement of 1-anilino-naphthalene 8-sulfonic acid. *Anal. Biochem.* **233**: 197–204.
14. Zhang, J., Z. P. Liu, T. A. Jones, L. M. Gierasch, and J. F. Sambrook.

1992. Mutating the charged residues in the binding pocket of cellular retinoic acid-binding protein simultaneously reduces its binding affinity to retinoic acid and increases its thermostability. *Proteins*. **13**: 87–99.
15. Richieri, G. V., R. T. Ogata, and A. M. Kleinfeld. 1995. Thermodynamics of fatty acid binding to fatty acid-binding proteins and fatty acid partition between water and membranes measured using the fluorescent probe ADIFAB. *J. Biol. Chem.* **270**: 15076–15084.
16. Kunkel, T. A. 1985. Rapid and efficient site-specific mutagenesis without phenotypic selection. *Proc. Natl. Acad. Sci. USA*. **82**: 488–492.
17. Ory, J., C. D. Kane, M. A. Simpson, L. J. Banaszak, and D. A. Bernlohr. 1997. Biochemical and crystallographic analyses of a portal mutant of the adipocyte lipid-binding protein. *J. Biol. Chem.* **272**: 9793–9801.
18. Rosenberg, A. H., B. N. Lade, D. Chui, S-W. Lin, J. J. Dunn, and F. W. Studier. 1987. Vectors for selective expression of cloned DNAs by T7 RNA polymerase. *Gene*. **56**: 125–135.
19. Schoepfer, R. 1993. The pRSET family of T7 promoter expression vectors for *Escherichia coli*. *Gene*. **124**: 83–85.
20. Johnson, B. H., and M. H. Hecht. 1994. Recombinant proteins can be isolated from *E. coli* cells by repeated cycles of freezing and thawing. *Bio/Technology*. **12**: 1357–1360.
21. Thompson, J. R., J. M. Bratt, and L. J. Banaszak. 1995. Crystal structure of cellular retinoic acid binding protein I shows increased access to the binding cavity due to formation of an intermolecular beta-sheet. *J. Mol. Biol.* **252**: 433–446.
22. Xu, Z. H., M. K. Buelt, L. J. Banaszak, and D. A. Bernlohr. 1991. Expression, purification, and crystallization of the adipocyte lipid binding protein. *J. Biol. Chem.* **266**: 14367–14370.
23. Glatz, J. F. C., and J. H. Veerkamp. 1983. A radiochemical procedure for the assay of fatty acid binding by proteins. *Anal. Biochem.* **132**: 89–95.
24. Glatz, J. F., and J. H. Veerkamp. 1983. Removal of fatty acids from serum albumin by Lipidex 1000 chromatography. *J. Biochem. Biophys. Methods*. **8**: 57–61.
25. LaLonde, J. M., D. A. Bernlohr, and L. J. Banaszak. 1994. X-ray crystallographic structures of adipocyte lipid-binding protein complexed with palmitate and hexadecanesulfonic acid. Properties of cavity binding sites. *Biochemistry*. **33**: 4885–4895.
26. LaLonde, J. M., M. A. Levenson, J. J. Roe, D. A. Bernlohr, and L. J. Banaszak. 1994. Adipocyte lipid-binding protein complexed with arachidonic acid. Titration calorimetry and X-ray crystallographic studies. *J. Biol. Chem.* **269**: 25339–25347.
27. Carter, C. W., Jr., and C. W. Carter. 1979. Protein crystallization using incomplete factorial experiments. *J. Biol. Chem.* **254**: 12219–12223.
28. Howard, A. J., G. L. Gilliland, B. C. Finzel, T. L. Poulos, D. H. Ohlendorf, and F. R. Salemme. 1987. The use of imaging proportional counter in macromolecular crystallography. *J. Appl. Crystallogr.* **20**: 383–387.
29. Rigaku. (1998) CrystalClear. Version 1.2.2. Rigaku/MSO, The Woodlands, TX.
30. Brünger, A. (1990) X-PLOR: A System for Crystallography and NMR. Version 3.1. Yale University Press, New Haven, CT.
31. Brünger, A. T., P. Adams, M. Clore, P. Gros, M. Nilges, and R. Read. 1998. Crystallography and NMR system. *Acta Crystallogr.* **D54**: 905–921.
32. Jones, T. A., J. Y. You, S. W. Cowan, and M. Kjeldgaard. 1991. Improved methods for building protein models in electron density maps and the location of errors in these models. *Acta Crystallogr.* **A47**: 110–119.
33. Kleywegt, G. J., and T. A. Jones. 1996. xdlMAPMAN and xdlDATAMAN—programs for reformatting, analysis and manipulation of biomacromolecular electron-density maps and reflection data sets. *Acta Crystallogr.* **D52**: 826–828.
34. Brünger, A. T. 1992. The free R value: a novel statistical quantity for assessing the accuracy of crystal structures. *Nature*. **355**: 472–474.
35. Laskowski, R. A., M. W. MacArthur, D. S. Moss, and J. M. Thornton. 1993. PROCHECK: a program to check the stereochemical quality of protein structures. *J. Appl. Crystallogr.* **26**: 283–291.
36. Liang, J., H. Edelsbrunner, and C. Woodward. 1998. Anatomy of protein pockets and cavities: measurement of binding site geometry and implications for ligand design. *Protein Sci.* **7**: 1884–1897.
37. Buelt, M. K., Z. Xu, L. J. Banaszak, and D. A. Bernlohr. 1992. Structural and functional characterization of the phosphorylated adipocyte lipid-binding protein (pp15). *Biochemistry*. **31**: 3493–3499.
38. Prinsen, C. F., and J. H. Veerkamp. 1996. Fatty acid binding and conformational stability of mutants of human muscle fatty acid-binding protein. *Biochem. J.* **314**: 253–260.
39. Kirk, W. R., E. Kurian, and F. G. Prendergast. 1996. Characterization of the sources of protein-ligand affinity: 1-sulfonato-8-(1')anilinonaphthalene binding to intestinal fatty acid binding protein. *Biophys. J.* **70**: 69–83.
40. Ong, D., and F. Chytil. 1978. Cellular retinoic acid-binding protein from rat testis: purification and characterization. *J. Biol. Chem.* **253**: 4551–4554.
41. Synergy Software. (2000) KaleidaGraph: Data Analysis and Graphic Presentation for Business, Science and Engineering. Version 3.5. Synergy Software, Reading, PA.
42. Simpson, M. A., and D. A. Bernlohr. 1998. Analysis of a series of phenylalanine 57 mutants of the adipocyte lipid-binding protein. *Biochemistry*. **37**: 10980–10986.
43. Epps, D. E., T. J. Raub, and F. J. Kedzy. 1995. A general, wide-range spectrofluorometric method for measuring the site-specific affinities of drugs toward human serum albumin. *Anal. Biochem.* **227**: 342–350.
44. MicroCal. 1993. ORIGIN. Version 2.9. MicroCal, Northampton, MA.
45. Brünger, A. T. 1990. Rigid body refinement reference. *Acta Crystallogr.* **A46**: 46–57.
46. Brünger, A. T. 1988. Crystallographic refinement by simulated annealing. Application to a 2.8 Å resolution structure of aspartate aminotransferase. *J. Mol. Biol.* **203**: 803–816.
47. Jiang, J. S., and A. T. Brünger. 1994. Protein hydration observed by X-ray diffraction. Solvation properties of penicillopepsin and neuraminidase crystal structures. *J. Mol. Biol.* **243**: 100–115.
48. Xu, Z., D. A. Bernlohr, and L. J. Banaszak. 1992. Crystal structure of recombinant murine adipocyte lipid-binding protein. *Biochemistry*. **31**: 3484–3492.
49. Ory, J. J., and L. J. Banaszak. 1999. Studies of the ligand binding reaction of adipocyte lipid binding protein using the fluorescent probe 1,8-anilinonaphthalene-8-sulfonate. *Biophys. J.* **77**: 1107–1116.
50. Predki, P. F., V. Agrawal, A. T. Brunger, and L. Regan. 1996. Amino-acid substitutions in a surface turn modulate protein stability. *Nat. Struct. Biol.* **3**: 54–58.
51. Lee, A. Y., P. Zhang, J. Clardy, B. Ganem, J. W. Erickson, and D. Xie. 1998. Thermodynamics of a transition state analogue inhibitor binding to *Escherichia coli* chorismate mutase: probing the charge state of an active site residue and its role in inhibitor binding and catalysis. *Biochemistry*. **37**: 9052–9057.
52. Mandiyan, V., R. O'Brien, M. Zhou, B. Margolis, M. A. Lemmon, J. M. Sturtevant, and J. Schlessinger. 1996. Thermodynamic studies of SHC phosphotyrosine interaction domain recognition of the NPXpY motif. *J. Biol. Chem.* **271**: 4770–4775.
53. Reddy, S. G., G. Scapin, and J. S. Blanchard. 1996. Interaction of pyridine nucleotide substrates with *Escherichia coli* dihydrodipicolinate reductase: thermodynamic and structural analysis of binary complexes. *Biochemistry*. **35**: 13294–13302.
54. Balendiran, G. K., F. Schnütgen, G. Scapin, T. Borchers, N. Xhong, K. Lim, R. Godbout, F. Spener, and J. C. Sacchittini. 2000. Crystal structure and thermodynamic analysis of human brain fatty acid-binding protein. *J. Biol. Chem.* **275**: 27045–27054.
55. LiCata, V. J., and D. A. Bernlohr. 1998. Surface properties of adipocyte lipid-binding protein: response to lipid binding, and comparison with homologous proteins. *Proteins*. **33**: 577–589.
56. Bernlohr, D. A., C. W. Angus, M. D. Lane, M. A. Bolanowski, and T. J. Kelly, Jr. 1984. Expression of specific mRNAs during adipose differentiation: identification of an mRNA encoding a homologue of myelin P2 protein. *Proc. Natl. Acad. Sci. USA*. **81**: 5468–5472.
57. Stoner, C. M., and L. J. Gudas. 1989. Mouse cellular retinoic acid binding protein: cloning, complementary DNA sequence, and messenger RNA expression during the retinoic acid-induced differentiation of F9 wild type and RA-3-10 mutant teratocarcinoma cells. *Cancer Res.* **49**: 1497–1504.
58. Evans, S. V. 1993. SETOR: hardware-lighted three-dimensional solid model representations of macro-molecules. *J. Mol. Graph.* **11**: 134–138.
59. Christopher, J. A. 1997. SPOCK. Texas A&M Center for Macromolecular Design, College Station, TX.
60. Wallace, A. C., R. A. Laskowski, and J. M. Thornton. 1995. LIGPLOT: a program to generate schematic diagrams of protein-ligand interactions. *Protein Eng.* **8**: 127–134.